PHOTONICS Research

Athermal 4-channel (de-)multiplexer in silicon nitride fabricated at low temperature

Shiqi Tao,[1] Qingzhong Huang,[1,2] Liangqiu Zhu,[1] Jun Liu,[1] Yinglu Zhang,[1] Ying Huang,[1] Yi Wang,[1] and Jinsong Xia[1,3]

[1]Wuhan National Laboratory for Optoelectronics, Huazhong University of Science and Technology, Wuhan 430074, China
[2]e-mail: huangqz@mail.hust.edu.cn
[3]e-mail: jsxia@hust.edu.cn

Received 1 February 2018; revised 19 April 2018; accepted 29 April 2018; posted 3 May 2018 (Doc. ID 321216); published 14 June 2018

We have designed and realized an athermal 4-channel wavelength (de-)multiplexer in silicon nitride (SiN). Minimized thermal sensitivity is achieved in a wide wavelength range by using wide and narrow waveguides with low and different thermal-optic coefficients in the two arms of Mach–Zehnder interferometers (MZIs). The SiN core layer and SiO_2 cladding layers are deposited by a low-temperature plasma-enhanced chemical vapor deposition process. The fabricated MZI filter exhibits a thermal sensitivity within ±2.0 pm/°C in a wavelength range of 55 nm to near 1300 nm. Then, an athermal (de-)multiplexer based on cascaded MZIs has been demonstrated with a crosstalk ≤−22 dB and a thermal sensitivity <4.8 pm/°C for all four channels, reduced by 77% compared to a conventional SiN (de-)multiplexer. Owing to the passive operation and compatibility with the CMOS back-end process, our devices have potential applications in 3D integration of photonics and electronics.

OCIS codes: (130.3120) Integrated optics devices; (130.7408) Wavelength filtering devices.

https://doi.org/10.1364/PRJ.6.000686

1. INTRODUCTION

In the past decades, silicon-based photonic integration has attracted great attention from the academia and industry [1–3], since it is compatible with CMOS processes and microelectronic circuits. For many applications, optical filters and (de-)multiplexers are essential components in the photonic integrated circuits [4–7]. However, a fundamental limitation of the silicon filtering devices is the high sensitivity to ambient temperature variation, due to the high thermo-optic coefficient (TOC) of silicon ($\sim 1.86 \times 10^{-4}$/°C) [8–10]. Hence, several approaches have been suggested to overcome this limitation. One approach is to dynamically heat the devices and compensate the shift using a feedback loop [11–14]. However, it consumes a large amount of power and requires substantial space. Another approach is to passively achieve thermal insensitivity by cladding the waveguides with negative TOC materials [15,16], but it is not CMOS compatible and reliable, and also complicates the fabrication. Then, a simple and passive approach is proposed based on asymmetric Mach–Zehnder interferometers (MZIs) [17,18], utilizing the interfering waveguides with different TOCs and carefully chosen lengths. For athermal silicon MZI filters, enormous progress has been made by using the difference between the two arms in the waveguide width [17–19], the waveguide type [20], the waveguide material [21], the polarization [22], or the mode order [23]. A typical thermal sensitivity is less than ±10 pm/°C over a wavelength range of 30 nm [24]. Recently, an athermal silicon (de-)multiplexer based on cascaded MZIs has been demonstrated with a crosstalk of −15 dB, and a thermal sensitivity <22 pm/°C for all the channels [25]. However, the reported performance is not very satisfying, due to inherent high TOC and stringent fabrication requirements of silicon waveguides.

Silicon nitride (SiN) is another common material in CMOS processes for masking, passivation, and dielectric layers [26,27]. Compared to silicon, SiN has a much lower TOC ($\sim 2.45 \times 10^{-5}$/°C) and a moderate index contrast, which can reduce the thermal sensitivity and relax the fabrication requirement [28]. Then, SiN layers can be deposited using either low-pressure chemical vapor deposition (LPCVD) or plasma-enhanced chemical vapor deposition (PECVD). Using LPCVD SiN waveguides with low loss, Dai *et al.* realized an array waveguide grating (de-)multiplexer with a thermal sensitivity of ~11 pm/°C [29], and recently Gao *et al.* have demonstrated a 4-channel (de)multiplexer based on cascaded conventional MZIs with a thermal sensitivity of ~18.5 pm/°C [30]. By combining slot and strip waveguides in the two arms, an athermal SiN MZI filter is achieved with a thermal sensitivity reduced to 5 pm/°C [31]. Thus, it is expected that the SiN (de-)multiplexer can be further optimized by cascading such MZIs. In recent years, PECVD SiN waveguide devices have

been of great interest. PECVD and LPCVD SiN waveguides have similar propagation loss in the O-band [32,33]. In contrast to LPCVD, PECVD waveguides are compatible with the CMOS backend process and more suitable for the 3D integration of photonics and electronics [32–35], due to the low-temperature fabrication (<400°C). Recently, a 3-channel (de-)multiplexer based on PECVD SiN waveguides has been realized with a thermal sensitivity less than 10 pm/°C [36]. However, the thermal sensitivity of this design merely depends on the TOC of deposited SiN, and can hardly be further reduced without active compensation or assisted materials.

In this paper, we have demonstrated an athermal SiN-based 4-channel wavelength (de-)multiplexer fabricated at low temperature. Due to the low TOC of SiN, the MZI filter combining wide and narrow waveguides exhibits a thermal sensitivity less than ±2.0 pm/°C over a wavelength range of 55 nm in the O-band. Consequently, by cascading such MZI structures, a low-crosstalk 4-channel wavelength (de-)multiplexer on a silicon substrate has been realized with a thermal sensitivity smaller than 4.8 pm/°C for all the channels, which is the best value reported, to the best of our knowledge. Our approach is simple, passive, and compatible with the standard CMOS process, leading to potential applications in the multilayer monolithic integration of photonics and electronics.

2. DEVICE STRUCTURE AND SIMULATION

It is known that the response of an MZI depends on the phase difference between two interfering arms and not the absolute phase shift. Here, to minimize the thermal sensitivity, a certain phase difference between the two arms is maintained by using wide and narrow waveguides with different TOCs and appropriate lengths in the two arms when the ambient temperature varies [19]. Figure 1 shows the schematics of the presented athermal MZI filter and 4-channel MZI (de-)multiplexer. As seen, there are three kinds of waveguides in the asymmetric MZIs: normal waveguides (width: W_1), wide waveguides (W_2), and narrow waveguides (W_3). All the splitters of MZIs are based on 2 × 2 multimode interference (MMI) couplers with a 50:50 splitting ratio. For the MZI filter shown in Fig. 1(a), the lengths of the wide and narrow waveguides are the same and denoted by L, while the total lengths of the normal waveguides in the upper and lower arms are different by $l = L_2 - L_1$. Then, in each arm, the wide/narrow waveguide and the normal waveguides are connected through identical linear tapers with a length of L_t. All the 90° bends in this structure have the same bending radius.

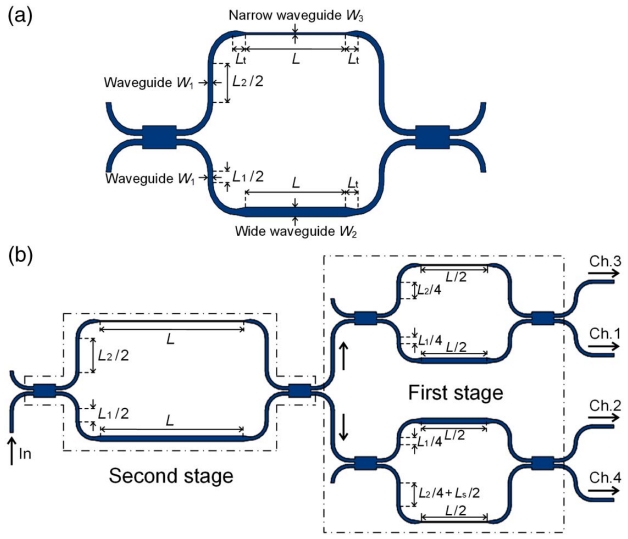

Fig. 1. Schematics of the athermal (a) MZI filter and (b) 4-channel MZI (de-)multiplexer.

Thus, the phase condition for the constructive interference at the wavelength λ is given by [19]

$$m\lambda = n_1 l + (n_3 - n_2)(L + L_t), \tag{1}$$

where m is an integer, representing the interference order, and n_i is the mode effective index (the subscripts $i = 1, 2, 3$ correspond to the normal, wide, and narrow waveguides, respectively).

Considering the wavelength dispersion, the thermal sensitivity of the MZI can be described by

$$\frac{d\lambda}{dT} = \frac{\frac{\partial n_1}{\partial T} l + \frac{\partial n_3 - \partial n_2}{\partial T}(L + L_t)}{m - \frac{\partial n_1}{\partial \lambda} l - \frac{\partial n_3 - \partial n_2}{\partial \lambda}(L + L_t)}, \tag{2}$$

where $\partial n_i/\partial T$ and n_{gi} are the TOC and group index of waveguide mode, respectively.

Then, the free spectral range (FSR) of the MZI is expressed as

$$\mathrm{FSR} \approx \frac{\lambda^2}{|n_{g1} l + (n_{g3} - n_{g2})(L + L_t)|}. \tag{3}$$

As shown in Fig. 1(b), the 4-channel (de-)multiplexer is based on cascaded athermal MZI filters. In this structure, the second-stage MZI separates the wavelength channels into two groups with an FSR equal to twice the channel spacing. Then, the first-stage MZI filters continue to separate the wavelength channels with an FSR equal to four times the channel spacing. To achieve four uniform channels, the lengths of the normal, wide, and narrow waveguides in the MZIs are set as illustrated in Fig. 1(b). It is seen that one arm of the lower first-stage MZI is modified by adding normal waveguide sections with a total length of $L_s = \lambda/(4n_1)$, since there is a $\pi/2$ phase difference in one arm of the two first-stage MZIs [37].

Here, SiN waveguides buried in SiO_2 with a fixed height of 400 nm are employed, as shown in the inset of Fig. 2(a). The finite element method is used to calculate the effective index

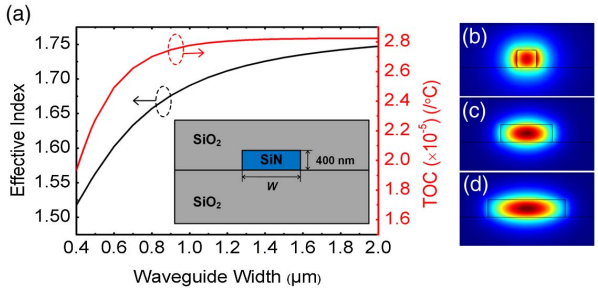

Fig. 2. (a) Simulated effective index and TOC of the TE_0 mode; inset: cross section of SiN waveguide. (b)–(d) Field profiles of the TE_0 mode for $W = 0.44$ μm, 1.2 μm, and 1.8 μm, respectively.

and TOC of the fundamental transverse-electric-like mode (TE_0) as a function of the waveguide width at 1300-nm wavelength. In our simulation, the refractive indices of SiN and SiO_2 are 1.981 and 1.446, respectively, which are the measured results of the SiN and SiO_2 films deposited by PECVD in our lab. The deposited SiN film is slightly N-rich. The TOC of SiO_2 is 1.0×10^{-5}/°C [10], while the TOC of SiN is estimated as 3.0×10^{-5}/°C, a little higher than that of stoichiometric SiN [36]. The simulation results using the setting values are in good agreement with our experiment. Figure 2(a) shows that both the effective index and TOC of the waveguiding mode increase monotonously with the waveguide width ranging from 0.4 μm to 2.0 μm. For compactness, the MZI requires a relatively large difference in TOC of the wide and narrow waveguides. In this work, we choose $W_1 = 1.2$ μm, $W_2 = 1.8$ μm, and $W_3 = 0.44$ μm. Hence, we can obtain $n_1 = 1.71$, $n_2 = 1.74$, $n_3 = 1.54$, $\partial n_1/\partial T = 2.81 \times 10^{-5}$/°C, $\partial n_2/\partial T = 2.82 \times 10^{-5}$/°C, and $\partial n_3/\partial T = 2.09 \times 10^{-5}$/°C. Compared to silicon, SiN waveguides have larger dimensions due to the moderate refractive index, and thus their phase error is smaller for a fixed fabrication error. Hence, the athermal SiN filters are more fabrication tolerant. The field profiles of TE_0 mode in waveguides are shown in Figs. 2(b)–2(d). It is seen that the field confinements in the SiN core of these waveguides are quite different. In our design, we choose $L_t = 20$ μm and bending radius of 60 μm to reduce the propagation loss in the tapered and curved waveguides. From Eq. (2), the condition $d\lambda/dT = 0$ should be satisfied to achieve athermal operation, indicating that the lengths of these waveguides need to be chosen carefully.

3. FABRICATION AND CHARACTERIZATION

To fabricate the SiN devices, we start with a clean bare silicon wafer. First, a 2-μm-thick SiO_2 layer was deposited on the wafer by PECVD at 300°C with mixture gas of SiH_4, N_2, and N_2O as the bottom cladding. Then, the SiN core layer of 400 nm in thickness was deposited on the SiO_2 layer by PECVD at 300°C using SiH_4, N_2, and NH_3. After that, the device patterns were defined in ZEP520A resist by electron-beam lithography, and subsequently transferred to the SiN layer by inductively coupled plasma etching technique with a depth of 400 nm. Finally, a PECVD SiO_2 layer was grown with a thickness of 1 μm as the top cladding of devices. It is seen that no high-temperature process is involved in the fabrication, and the deposited films are stress free and can be thicker if needed. Therefore, the design of the proposed devices is flexible, and the fabrication is quite suitable for the CMOS backend process.

Figure 3(a) illustrates an optical microscope image of the fabricated 4-channel MZI (de-)multiplexer. Many parts of the device are shown in detail by the scanning electron microscope (SEM) images in Figs. 3(b)–3(e) before the top layer is deposited. Here, the footprint of the 2 × 2 MMI is 6 μm × 34 μm. The taper length L_t is 20 μm, and the bending radius is 60 μm for negligible radiation losses in the tapered and curved waveguides. The total footprint of the fabricated athermal SiN (de-)multiplexer is about 1.73 mm × 0.76 mm. To characterize the SiN waveguide devices, a broadband amplified spontaneous emission source is employed. TE-polarized light is obtained utilizing an optical polarizer and a polarization controller, and then coupled into the chip through a grating coupler. A thermal-electric cooler equipped sample stage is used to control the temperature of the device under test. Finally, the transmitted light from the device is coupled out through another grating coupler and collected by a fiber connected to the optical spectrum analyzer or optical power meter.

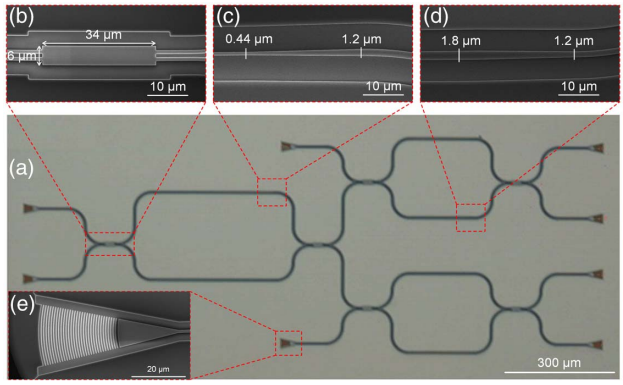

Fig. 3. (a) Optical microscope image of the athermal 4-channel (de-)multiplexer. SEM images of (b) a 2 × 2 MMI, (c) narrow waveguide and normal waveguide connected by a taper, (d) wide waveguide and normal waveguide connected by a taper, and (e) grating coupler for vertical coupling.

4. EXPERIMENTAL RESULTS

A. Athermal MZI Filter

It is known from Eq. (2) that the thermal sensitivity of MZI is highly dependent on L. Hence, we fabricated MZI filters with different L, while other structural parameters are maintained, including $l = 120$ μm. The normalized transmission spectra of the MZI filters under different temperatures for $L = 410$ μm, 430 μm, 450 μm, and 470 μm are shown in Figs. 4(a)–4(d), respectively. It is observed that the spectral shifts with temperature for these devices are relatively small, because of the athermal design and low TOC of SiN. The transmission spectrum is slightly red shifted for $L = 410$ μm and 430 μm, while it is blue shifted for $L = 450$ μm and 470 μm, as the temperature increases from 30°C to 50°C. Figure 4(e) shows the transmission spectrum for the MZI filter with $L = 450$ μm in a broad wavelength range. The averaged on-chip insertion loss of this filter is about 2.6 dB. It is noteworthy that minor spectral shift with temperature is seen over an 80-nm wavelength span from 1260 nm to 1340 nm.

Figure 5(a) shows the dependence of thermal sensitivity on L for the MZI filter. The experimental results agree well with the theoretical simulations. The thermal sensitivity varies from positive to negative as L increases. It is expected that athermal operation can be achieved for the MZI filter with L of around 440 μm. The slightly nonlinear $d\lambda/dT$-L curve results from the wavelength dependence of the TOCs of SiN waveguides. Figure 5(b) shows the measured thermal sensitivity as a function of wavelength extracted from the results in Fig. 4(e), which is generally consistent with the theoretical curve. A thermally

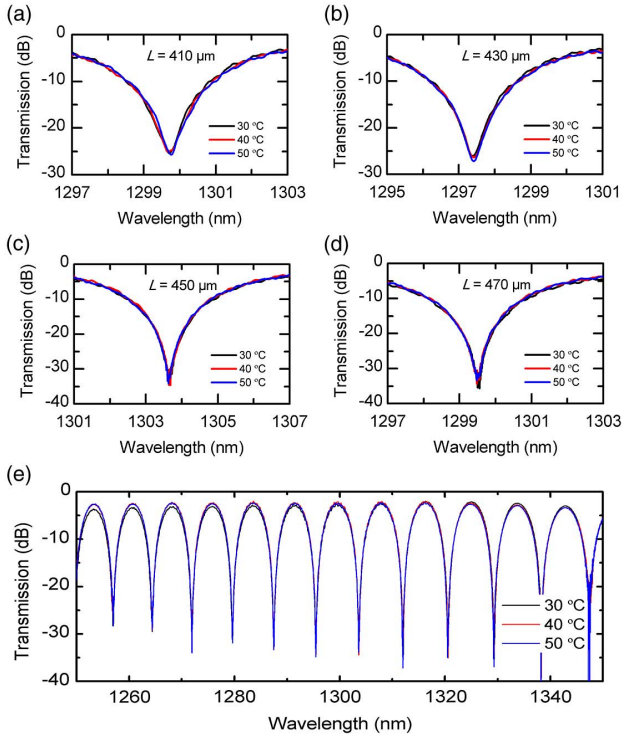

Fig. 4. Transmission spectra of MZI filters at different temperatures for (a) $L = 410$ μm, (b) $L = 430$ μm, (c) $L = 450$ μm, and (d) $L = 470$ μm. (e) Wide transmission spectrum of the MZI filter with $L = 450$ μm.

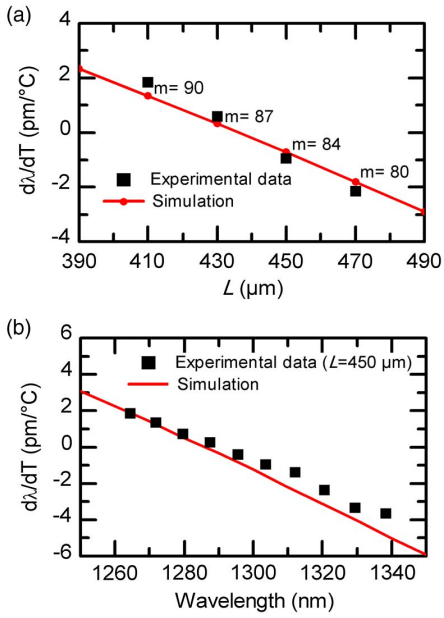

Fig. 5. (a) Thermal sensitivity as a function of L. (b) Thermal sensitivity as a function of wavelength.

insensitive MZI filter is demonstrated with a thermal sensitivity within ±2.0 pm/°C in a wavelength range of 55 nm to near 1300 nm. The thermal sensitivity decreases with wavelength, since the optical confinement in the SiN waveguide is reduced

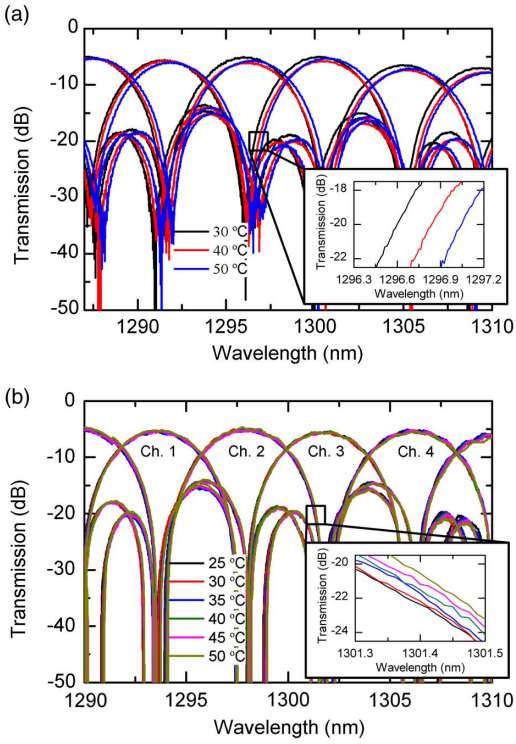

Fig. 6. Measured normalized transmission spectra of (a) conventional MZI (de-)multiplexer and (b) athermal MZI (de-)multiplexer.

Table 1. Room-Temperature Performance of the Athermal MZI (De-)Multiplexer

	Ch. 1	Ch. 2	Ch. 3	Ch. 4
Center wavelength (nm)	1293.6	1297.7	1301.9	1306.1
Crosstalk at center (dB)	−30	−25	−22	−23
1-dB bandwidth (nm)	2.2	2.2	2.2	2.2
Insertion loss (dB)	5.5	5.2	5.5	5.5
Channel spacing (nm)	4.3	4.0	4.2	

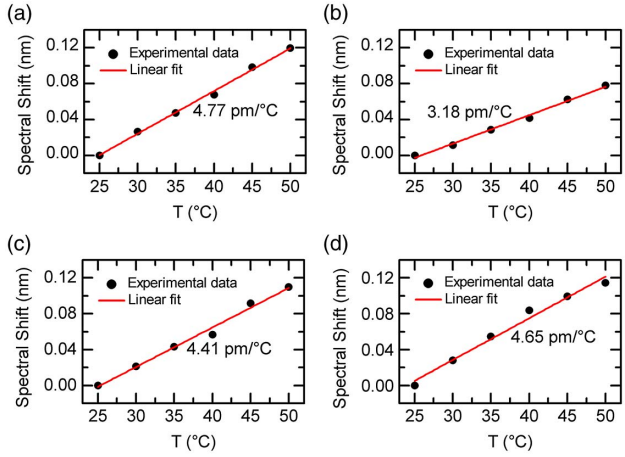

Fig. 7. Spectral shift with temperature for (a) Ch. 1, (b) Ch. 2, (c) Ch. 3, and (d) Ch. 4.

Table 2. Performance Comparison of the MZI Filters and (De-)Multiplexers with Low Thermal Sensitivity (MUX, multiplexer; IL, insertion loss; ET, extinction ratio for MZI filter; XT, crosstalk for MUX)

Ref.	Material	Device	$d\lambda/dT$ (pm/°C)	IL (dB)	ET/XT (dB)
Dwivedi *et al.* [22]	Silicon	MZI filter	<±15 (in 40 nm)	0.3	−25
Yang *et al.* [24]	Silicon	MZI filter	<±10 (in 30 nm)	N.A.	−30
Xing *et al.* [23]	Silicon	MZI filter	<±2.5 (in 60 nm)	1	−10
Our device	SiN (PECVD)	MZI filter	<±2.0 (in 55 nm)	2.6	−30
Hassan *et al.* [25]	Silicon	MZI MUX 4	< 22 (all channels)	4.3	−15
Gao *et al.* [30]	SiN (LPCVD)	MZI MUX 4	18.7 (central channel)	1.8	−20
Bucio *et al.* [36]	SiN (PECVD)	AMMI MUX 3	10 (central channel)	2.5	−18
Our device	SiN (PECVD)	MZI MUX 4	<4.8 (all channels)	5.5	−22

as the wavelength increases [38]. For the central channel of a silicon MZI filter, recently, Hiraki *et al.* have achieved a thermal sensitivity of −2.8 pm/°C by changing the TOCs of the waveguide materials [21], and Lee *et al.* have obtained a thermal sensitivity less than 2.0 pm/°C by combining wide and narrow waveguides [39]. However, the thermal sensitivity will increase as the wavelength moves away from the central channel. For example, Dwivedi *et al.* have shown that the thermal sensitivity of a silicon MZI filter increases to ∼15 pm/°C as the wavelength shift is 20 nm [22]. Owing to the low TOC of SiN, our MZI filter exhibits a minimum thermal sensitivity of 0.6 pm/°C, while the thermal sensitivity is still less than 2 pm/°C for a wavelength shift of 25 nm.

B. Athermal 4-Channel (De-)Multiplexer

Consequently, we fabricated a 4-channel SiN (de-)multiplexer by cascading the MZIs according to the previous design of MZI filters in order to achieve athermal operation. The approach has been described in Section 2. Then, for comparison, we also fabricated a conventional 4-channel SiN MZI (de-)multiplexer based on normal waveguides. Figures 6(a) and 6(b) show the normalized transmission spectra of the conventional and athermal MZI (de-)multiplexers at different temperatures, respectively. It is found that their spectra are both red shifted, while the spectrum shapes remain the same, as the temperature increases from 25°C to 50°C. The measured thermal sensitivity is 21.29 pm/°C for the conventional 4-channel MZI (de-)multiplexer, consistent with the theoretical prediction for this N-rich SiN based (de-)multiplexer. In contrast, the thermal shift for the athermal (de-)multiplexer is much smaller. Table 1 summarizes the performance characteristics of the athermal (de-)multiplexer at room temperature (25°C). The crosstalk is below −22 dB for all four channels. The 1-dB bandwidth is 2.2 nm, which accounts for 52.8% of the channel spacing. The relatively large insertion loss of 5.2–5.5 dB is mainly attributed to the 3.96-dB loss in the MMIs (0.99 dB for each MMI), whereas the loss in strip waveguides is only 1.3–1.5 dB. Here, the propagation loss in a normal waveguide is 4.32 dB/cm. It indicates that the insertion loss of our device can be further reduced greatly if the MMI splitters are optimized. The channel spacing is 4.0–4.3 nm, and the nonuniformness is possibly caused by the phase error induced by the imperfect MMI couplers [40] and the enlarged group velocity dispersion of waveguides in a wide spectral range.

Figures 7(a)–7(d) illustrate the spectral shift with temperature for all four channels of the athermal MZI (de-)multiplexer. The thermal sensitivities are obtained by linear fitting the experimental results. The minimum thermal sensitivity is only 3.18 pm/°C for Ch. 2, and the thermal sensitivity is smaller than 4.8 pm/°C for all four channels, reduced by 77% compared to a conventional SiN (de-)multiplexer. To implement 4-channel (de-)multiplexing, we have cascaded multiple MZI filters with different FSRs. Then, for athermal operation, the optimized structure of each MZI filter is quite different. Thus, compared to an MZI filter, the 4-channel (de-)multiplexer is much larger, more complicated, and more sensitive to the fabrication errors. As a result of the non-ideally fabricated structure, the thermal sensitivity of our 4-channel (de-)multiplexer is larger than that of 2-channel MZIs. Table 2 summarizes the performance of the reported athermal MZI filters and (de-)multiplexers for comparison. It is seen that our thermal sensitivity is the smallest for either the MZI filter or (de-)multiplexer, owing to the low TOC of SiN waveguides and athermal design. It is the first demonstration of an athermal MZI (de-)multiplexer in SiN using a passive thermal compensation method. In addition, our devices are advantageous for low-temperature fabrication and compatible with the post-CMOS process.

5. CONCLUSION

In summary, we have demonstrated an athermal SiN (de-)multiplexer based on asymmetric MZIs with a combination of wide and narrow waveguides. The MZI filter exhibits a thermal sensitivity within ±2.0 pm/°C over a wavelength range of 55 nm to near 1300 nm. By cascading the athermal MZIs, we have realized an athermal 4-channel MZI (de-)multiplexer with a crosstalk ≤ −22 dB and a thermal sensitivity <4.8 pm/°C for all the channels. The waveguiding and cladding layers of devices are grown on a silicon substrate by low-temperature PECVD, which is post-CMOS compatible. It is expected that the proposed athermal devices will find potential applications in high-density optoelectronic integrated circuits.

Funding. 863 Program (2015AA016904); National Natural Science Foundation of China (NSFC) (61335002, 11574102, 61675084, 61775094).

Acknowledgment. The authors thank all the engineers in the Center of Micro-Fabrication and Characterization (CMFC) of Wuhan National Laboratory for Optoelectronics (WNLO) for the support in device fabrication.

REFERENCES

1. L. Pavesi and D. J. Lockwood, *Silicon Photonics* (Springer-Verlag, 2004).
2. R. Soref, "The past, present, and future of silicon photonics," IEEE J. Sel. Top. Quantum Electron. **12**, 1678–1687 (2006).
3. L. Thylеén and L. Wosinski, "Integrated photonics in the 21st century," Photon. Res. **2**, 75–81 (2014).
4. Q. Huang, X. Zhang, J. Xia, and J. Yu, "Dual-band optical filter based on a single microdisk resonator," Opt. Lett. **36**, 4494–4496 (2011).
5. Q. Huang, Q. Liu, and J. Xia, "Traveling wave-like Fabry–Perot resonator-based add-drop filters," Opt. Lett. **42**, 5158–5161 (2017).
6. S. Chen, Y. Shi, S. He, and D. Dai, "Compact monolithically-integrated hybrid (de)multiplexer based on silicon-on-insulator nanowires for PDM-WDM systems," Opt. Express **23**, 12840–12849 (2015).
7. Y. Li, Y. Zhang, L. Zhang, and A. W. Poon, "Silicon and hybrid silicon photonic devices for intra-datacenter applications: state of the art and perspectives [invited]," Photon. Res. **3**, B10–B27 (2015).
8. Y. P. Varshni, "Temperature dependence of the energy gap in semiconductors," Physica **34**, 149–154 (1967).
9. Q. Deng, X. Li, Z. Zhou, and H. Yi, "Athermal scheme based on resonance splitting for silicon-on-insulator microring resonators," Photon. Res. **2**, 71–74 (2014).
10. Q. Huang, K. Jie, Q. Liu, Y. Huang, Y. Wang, and J. Xia, "Ultra-compact, broadband tunable optical bandstop filters based on a multimode one-dimensional photonic crystal waveguide," Opt. Express **24**, 20542–20553 (2016).
11. S. Manipatruni, R. K. Dokania, B. Schmidt, N. Sherwood-Droz, C. B. Poitras, A. B. Apsel, and M. Lipson, "Wide temperature range operation of micrometer-scale silicon electro-optic modulators," Opt. Lett. **33**, 2185–2187 (2008).
12. H. Yu, M. Pantouvaki, S. Dwivedi, P. Verheyen, G. Lepage, R. Baets, W. Bogaerts, and J. Van Campenhout, "Compact thermally tunable silicon racetrack modulators based on an asymmetric waveguide," IEEE Photon. Technol. Lett. **25**, 159–162 (2013).
13. C. Sun, M. T. Wade, Y. Lee, J. S. Orcutt, L. Alloatti, M. S. Georgas, A. S. Waterman, J. M. Shainline, R. R. Avizienis, S. Lin, B. R. Moss, R. Kumar, F. Pavanello, A. H. Atabaki, H. M. Cook, A. J. Ou, J. C. Leu, Y.-H. Chen, K. Asanović, R. J. Ram, M. A. Popović, and V. M. Stojanović, "Single-chip microprocessor that communicates directly using light," Nature **528**, 534–538 (2015).
14. L. Lu, L. Zhou, X. Sun, J. Xie, Z. Zou, H. Zhu, X. Li, and J. Chen, "CMOS-compatible temperature-independent tunable silicon optical lattice filters," Opt. Express **21**, 9447–9456 (2013).
15. J. Teng, P. Dumon, W. Bogaerts, H. Zhang, X. Jian, X. Han, M. Zhao, G. Morthier, and R. Baets, "Athermal Silicon-on-insulator ring resonators by overlaying a polymer cladding on narrowed waveguides," Opt. Express **17**, 14627–14633 (2009).
16. B. Guha, J. Cardenas, and M. Lipson, "Athermal silicon microring resonators with titanium oxide cladding," Opt. Express **21**, 26557–26563 (2013).
17. M. Uenuma and T. Moooka, "Temperature-independent silicon waveguide optical filter," Opt. Lett. **34**, 599–601 (2009).
18. Z. Zhou, B. Yin, Q. Deng, X. Li, and J. Cui, "Lowering the energy consumption in silicon photonic devices and systems [invited]," Photon. Res. **3**, B28–B46 (2015).
19. B. Guha, A. Gondarenko, and M. Lipson, "Minimizing temperature sensitivity of silicon Mach–Zehnder interferometers," Opt. Express **18**, 1879–1887 (2010).
20. Q. Deng, L. Liu, R. Zhang, X. Li, J. Michel, and Z. Zhou, "Athermal and flat-topped silicon Mach–Zehnder filters," Opt. Express **24**, 29577–29582 (2016).
21. T. Hiraki, H. Fukuda, K. Yamada, and T. Yamamoto, "Small sensitivity to temperature variations of Si-photonic Mach–Zehnder interferometer using Si and SiN waveguides," Front. Mater. **2**, 1–5 (2015).
22. S. Dwivedi, H. D'heer, and W. Bogaerts, "Maximizing fabrication and thermal tolerances of all-silicon FIR wavelength filters," IEEE Photon. Technol. Lett. **27**, 871–874 (2015).
23. P. Xing and J. Viegas, "Broadband CMOS-compatible SOI temperature insensitive Mach–Zehnder interferometer," Opt. Express **23**, 24098–24107 (2015).
24. H. Yang, J. Zhang, Y. Zhu, X. Zhou, S. He, and L. Liu, "Ultra-compact and temperature-insensitive Mach–Zehnder interferometer based on one multimode waveguide on silicon," Opt. Lett. **42**, 615–618 (2017).
25. K. Hassan, C. Sciancalepore, J. Harduin, T. Ferrotti, S. Menezo, and B. B. Bakir, "Toward athermal silicon-on-insulator (de)multiplexers in the O-band," Opt. Lett. **40**, 2641–2644 (2015).
26. A. Rahim, E. Ryckeboer, A. Z. Subramanian, S. Clemmen, B. Kuyken, A. Dhakal, A. Raza, A. Hermans, M. Muneeb, S. Dhoore, Y. Li, U. Dave, P. Bienstman, N. Le Thomas, G. Roelkens, D. Van Thourhout, P. Helin, S. Severi, X. Rottenberg, and R. Baets, "Expanding the silicon photonics portfolio with silicon nitride photonic integrated circuits," J. Lightwave Technol. **35**, 639–649 (2017).
27. A. Z. Subramanian, E. Ryckeboer, A. Dhakal, F. Peyskens, A. Malik, B. Kuyken, H. Zhao, S. Pathak, A. Ruocco, A. De Groote, P. Wuytens, D. Martens, F. Leo, W. Xie, U. D. Dave, M. Muneeb, P. Van Dorpe, J. Van Campenhout, W. Bogaerts, P. Bienstman, N. Le Thomas, D. Van Thourhout, Z. Hens, G. Roelkens, and R. Baets, "Silicon and silicon nitride photonic circuits for spectroscopic sensing on-a-chip [invited]," Photon. Res. **3**, B47–B59 (2015).
28. A. Arbabi and L. L. Goddard, "Measurements of the refractive indices and thermo-optic coefficients of Si_3N_4 and SiO_x using microring resonances," Opt. Lett. **38**, 3878–3881 (2013).
29. D. Dai, Z. Wang, J. F. Bauters, M. C. Tien, M. J. Heck, D. J. Blumenthal, and J. E. Bowers, "Low-loss Si_3N_4 arrayed-waveguide grating (de)multiplexer using nano-core optical waveguides," Opt. Express **19**, 14130–14136 (2011).
30. G. Gao, D. Chen, S. Tao, Y. Zhang, S. Zhu, X. Xiao, and J. Xia, "Silicon nitride O-band (de) multiplexers with low thermal sensitivity," Opt. Express **25**, 12260–12267 (2017).
31. X. Tu, J. F. Song, T.-Y. Liow, M. K. Park, J. Q. Yiying, J. S. Kee, M. B. Yu, and G. Q. Lo, "Thermal independent silicon-nitride slot waveguide biosensor with high sensitivity," Opt. Express **20**, 2640–2648 (2012).
32. Y. Huang, J. Song, X. Luo, T.-Y. Liow, and G.-Q. Lo, "CMOS compatible monolithic multi-layer Si_3N_4-on-SOI platform for low-loss high performance silicon photonics dense integration," Opt. Express **22**, 21859–21865 (2014).
33. W. Sacher, Y. Huang, G. Lo, and J. Poon, "Multilayer silicon nitride-on-silicon integrated photonic platforms and devices," J. Lightwave Technol. **33**, 901–910 (2015).
34. N. Sherwood-Droz and M. Lipson, "Scalable 3D dense integration of photonics on bulk silicon," Opt. Express **19**, 17758–17765 (2011).
35. Z. Zhang, B. Huang, X. Zhang, Z. Zhang, C. Cheng, X. Mao, S. Liu, and H. Chen, "Monolithic integration of Si_3N_4 microring filters with bulk CMOS IC through post-backend process," IEEE Photon. Technol. Lett. **27**, 1543–1546 (2015).
36. T. D. Bucio, A. Z. Khokhar, G. Z. Mashanovich, and F. Y. Gardes, "Athermal silicon nitride angled MMI wavelength division (de)multiplexers for the near-infrared," Opt. Express **25**, 27310–27320 (2017).
37. F. Horst, W. M. J. Green, S. Assefa, S. M. Shank, Y. A. Vlasov, and B. J. Offrein, "Cascaded Mach–Zehnder wavelength filters in silicon photonics for low loss and flat pass-band WDM (de-)multiplexing," Opt. Express **21**, 11652–11658 (2013).
38. V. Raghunathan, T. Izuhara, J. Michel, and L. C. Kimerling, "Stability of polymer-dielectric bi-layers for athermal silicon photonics," Opt. Express **20**, 16059–16066 (2012).
39. J.-M. Lee, M.-S. Kim, M. Fournier, P. Labeye, C. J. Oton, and F. Testa, "Postfabrication trimming of CMOS-compatible athermal MZI by thermal annealing," J. Lightwave Technol. **34**, 1288–1292 (2016).
40. J. Z. Huang, R. Scarmozzino, and R. M. Osgood, Jr., "A new design approach to large input/output number multimode interference couplers and its application to low-crosstalk WDM routers," IEEE Photon. Technol. Lett. **10**, 1292–1294 (1998).